ARTICLE IN PRESS

Magnetic Resonance Imaging xxx (2015) xxx–xxx

Contents lists available at ScienceDirect

Magnetic Resonance Imaging

journal homepage: www.mrijournal.com

Original contribution

Selection of magnetization catalyzation and readout methods for modified Look–Locker inversion recovery: A T_1 mapping primer

Donnie Cameron [a,*], David M. Higgins [b], Christian Stehning [c], Marc Kouwenhoven [d], Mustapha Bouhrara [e], Michael P. Frenneaux [a], Dana K. Dawson [a,1], Thomas W. Redpath [a,1]

[a] The University of Aberdeen, Aberdeen, UK
[b] Philips Healthcare, Guildford, Surrey, UK
[c] Philips Research, Hamburg, Germany
[d] Philips Healthcare, Best, The Netherlands
[e] National Institute on Aging, National Institutes of Health, Baltimore, MD, USA

ARTICLE INFO

Article history:
Received 20 November 2014
Revised 15 January 2015
Accepted 1 February 2015
Available online xxxx

Keywords:
T_1 mapping
Tissue characterization
Steady-state free precession
Transient signal oscillations

ABSTRACT

Background: The purpose of this work was to evaluate different magnetization preparation and readout sequences for modified Look–Locker inversion recovery (MOLLI) toward improved T_1 mapping in the heart. Elements investigated include: catalyzation sequences to prepare the magnetization before readout, alternate k-space trajectories, a spoiled gradient recalled echo readout, and a 5b(3b)3b MOLLI sampling scheme ('b' denoting beats).
Methods: Conventional 3b(3b)3b(3b)5b MOLLI with a linear k-space trajectory was compared to four variants in simulations, *in vitro* and *in vivo* (at 3T). Variants were centric conventional MOLLI, centric-paired conventional MOLLI, linear 5b(3b)3b MOLLI and spoiled gradient recalled echo MOLLI. Each of these was applied with three magnetization catalyzation methods, and T_1 measurement accuracy and precision were evaluated in simulations via a Monte Carlo algorithm, in a set of calibrated phantoms, and in ten healthy volunteers. Contrast-to-noise, heart rate dependence and B_1+ dependence were also evaluated.
Results: A linear k-space trajectory was superior *in vitro* to centric and centric-paired trajectories. Of the catalyzation methods, preparation of transverse magnetization only—using a linearly increasing flip angle catalyzation—improved MOLLI T_1 measurement accuracy, precision, and map quality versus methods that include catalyzation of the longitudinal magnetization. The 5b(3b)3b MOLLI scheme offered comparable native T_1 measurement accuracy and precision to conventional MOLLI, despite its shortened acquisition.
Conclusions: MOLLI T_1 measurement accuracy, precision, and map quality depend on the method of catalyzation of magnetization prior to image acquisition, as well as on the readout method and MOLLI sampling scheme used.

1. Introduction

The modified Look–Locker inversion recovery (MOLLI) pulse sequence is used to measure the longitudinal relaxation time, T_1, in the beating heart. This allows for the quantitative assessment of myocardial T_1 values under both native and contrast-enhanced conditions. The original MOLLI sequence, [1] introduced in 2004 and further improved in Messroghli et al. [2], provides precise estimates of T_1 in myocardium; however, its T_1 measurement accuracy is suboptimal, and can be affected by numerous factors [3]. We propose that MOLLI can be altered to enhance its T_1 measurement utility via alternative k-space trajectories, different magnetization catalyzation sequences, and alternative readout methods—three topics that have seen little-to-no investigation in the literature, and will be discussed at length in this work.

1.1. Theory

Conventional MOLLI consists of multiple inversion recovery (IR) experiments, during which recovery of the longitudinal

* Corresponding author at: NIA, Harbor Hospital, 3001 Hanover Street, Baltimore, MD 21225, United States. Tel./fax: +1 410 350 7349/7304.
E-mail addresses: d.cameron.09@aberdeen.ac.uk (D. Cameron), david.higgins@philips.com (D.M. Higgins), christian.stehning@philips.com (C. Stehning), marc.kouwenhoven@philips.com (M. Kouwenhoven), mustapha.bouhrara2@nih.gov (M. Bouhrara), m.p.frenneaux@abdn.ac.uk (M.P. Frenneaux), dana.dawson@abdn.ac.uk (D.K. Dawson), t.redpath@abdn.ac.uk (T.W. Redpath).
[1] Equal contributors.

http://dx.doi.org/10.1016/j.mri.2015.02.004
0730-725X/© 2015 Elsevier Inc. All rights reserved.

magnetization is rapidly sampled using the Look–Locker technique [4]. An electrocardiogram-triggered, balanced steady-state free precession (bSSFP) readout is used for sampling during the cardiac cycle's most quiescent phase [5]. Due to timing constraints, data are acquired in the transient phase of the SSFP signal evolution, resulting in signal oscillations at the onset of the radiofrequency (RF) pulse train. These oscillations may produce spurious signal measurements, affecting the accuracy and precision of MOLLI T_1 estimates. A suitable magnetization catalyzation sequence for bSSFP—a linear flip angle sweep or a half-alpha (HA) approach, [6,7] for example—is essential for mitigating these oscillations. Several catalyzation sequences exist for preparing, or "priming", longitudinal and transverse magnetizations: typically a binomial RF pulse and spoiler gradients for the former, and a variable flip angle pulse train for the latter [8]. An example of a combined longitudinal and transverse magnetization catalyzation sequence is shown in Fig. 1. To date, the significance of catalyzation sequences to T_1 mapping is still in need of investigation.

Signal oscillations in bSSFP result in artifacts, and are associated with k-space ordering schemes [9]. While the improved 2007 MOLLI sequence used a centric k-space trajectory, [2] some MOLLI implementations—such as the original description in 2004—have used a linear trajectory to minimize signal oscillations [1]. However, with linear ordering, some saturation of the longitudinal magnetization occurs prior to sampling of the center of k-space. This acts as a k-space filter that results in underestimation of the transient longitudinal magnetization, degrading measurement accuracy. Centric ordering provides an estimate of M_z closer to the undisturbed-recovery case, though eddy currents are induced by large changes in gradient amplitude between phase encoding steps, causing signal variations that may reduce T_1 measurement accuracy. A compromise between linear and centric trajectories is the centric-paired approach, which mitigates such signal variations by pairing k-space samples according to the phase-alternating RF scheme of bSSFP [10]. Within these pairs, the dephasing generated by the first step is intrinsically canceled by the second step, and residual eddy currents are eliminated if their time-constants are longer than the repetition time (TR).

Conventional MOLLI uses a bSSFP readout for its high signal-to-noise ratio (SNR), high efficiency, and intrinsic flow compensation. However, this readout increases sensitivity to off-resonance, and some magnetization saturation occurs due to the moderate flip-angles (e.g. 20–35°) used to sample the recovering longitudinal magnetization—perturbing the recovery from the model assumed for T_1 calculation. The Look–Locker correction used in T_1 mapping requires two important assumptions: first, that the RF pulses used to sample longitudinal recovery are of low flip angle—less than 10° [11]—and secondly, that a continuous readout pulse train is applied. Neither assumption holds true for MOLLI, leading to substantial scope for error in its T_1 measurements [12]. The spoiled gradient recalled echo (GRE) readout, [13] a possible alternative to bSSFP, uses low flip angle excitation pulses, which cause less saturation in myocardium than the conventional MOLLI bSSFP readout, at the cost of a lower SNR. Such a readout may offer improved MOLLI T_1 measurement accuracy.

1.2. Aims

Previous studies have investigated the effect of heart rate, inversion time and inversion efficiency on MOLLI's accuracy and precision, [2,12,14,15] and recent works have evaluated these qualities in the context of extracellular volume measurements [16]. The primary aim in this study was to investigate several novel MOLLI variants—each based on a conventional 3b(3b)3b(3b)5b MOLLI scheme—with alternative magnetization catalyzations and image readouts. These were compared with conventional MOLLI, and the recently-reported 5b(3b)3b MOLLI, [15] in order to evaluate any improvements over the original MOLLI scheme. Comparisons were made via numerical simulations and *in vitro* and *in vivo* acquisitions, focusing on their heart rate dependence, B_1+ sensitivity, contrast-to-noise, and T_1 measurement accuracy and precision. Whether 3b(3b)3b(3b)5b MOLLI is an optimal scheme is not under investigation; readout effects within a chosen scheme are of interest here. It is anticipated that this work will inform users of other MOLLI schemes as well as users of the original method.

2. Materials and methods

All *in vitro* and *in vivo* experiments were performed on a three tesla MRI scanner (Achieva 3.0 T TX, Philips Healthcare, Best, The Netherlands) using a six-channel phased array cardiac coil for reception and two RF transmit channels—to improve B_1+ homogeneity via RF shimming [17,18].

A set of 7 doped agarose gel phantoms was prepared for this study, with T_1/T_2 values (in ms) as follows: 326/59, 470/57, 755/57, 876/64, 1110/59, 1227/58 and 1585/60. The T_1 range was chosen to cover native/post-contrast myocardium—post-contrast T_1 values being of interest for extracellular volume calculations [19]—and T_2 values were strictly controlled to minimize T_2 bias. Blood-like T_1 values were not included, as stationary phantoms are inadequate for assessment of flowing blood [15]. Phantom T_1 values were calibrated using an IR fast-spin-echo (IR-SE) sequence (TR/echo time [TE] = 10,000/12 ms; 11 inversion times, TI = 50:150:1100, 1400, 3000, and 5000 ms; in-plane resolution = 1.7 mm × 2.1 mm; slice thickness = 10 mm; echo train length = 6). All phantom experiments were performed at 21 °C.

2.1. Experimental setup

"Conventional MOLLI", based on the optimized original MOLLI sequence, [2] was chosen as a standard for comparisons—to evaluate

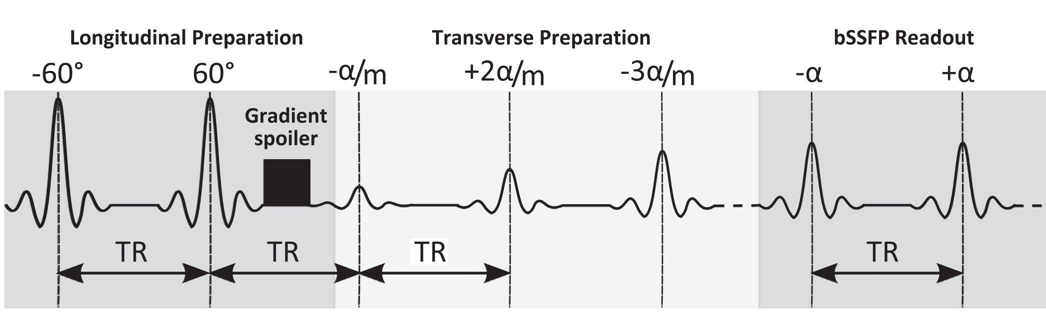

Fig. 1. Illustration of an LSUB magnetization catalyzation sequence for bSSFP: The sequence consists of longitudinal and transverse magnetization preparations, played prior to the bSSFP readout, with TR being the bSSFP TR. Note that the LSU catalyzation sequence described in this work omits the longitudinal preparation.

Please cite this article as: Cameron D, et al, Selection of magnetization catalyzation and readout methods for modified Look–Locker inversion recovery: A T_1 mapping primer, Magn Reson Imaging (2015), http://dx.doi.org/10.1016/j.mri.2015.02.004

any improvements relative to this widely reported method. The sequence consisted of three IR blocks, in a 3b(3b)3b(3b)5b arrangement, with b's indicating images were acquired one-per-beat, with a three beat pause between consecutive IR blocks. Other parameters were as follows: diastolic image acquisition, $\alpha = 35°$, TR/TE = 2.3/1.08 ms, in-plane resolution = 1.25×1.25 mm^2, matrix size = 288×288, a linear k-space trajectory, minimum TI = 100 ms, and a sensitivity encoding (SENSE) factor of 2. Four variants of this sequence were devised with the following modifications:

(A) A 5b(3b)3b MOLLI scheme with two IR blocks rather than three, as reported by Kellman and Hansen [15].
(B) A centric k-space trajectory.
(C) A centric-paired k-space trajectory.
(D) A spoiled GRE readout with an alpha-pulse flip angle of 4°—calculated as the Ernst angle for native myocardium [20].

Each MOLLI variant was otherwise identical to conventional MOLLI. All five MOLLI sequences (besides spoiled GRE) were tested with three popular cardiac magnetization catalyzation sequences in simulations, *in vitro* and *in vivo*, as follows:

(i) An HA catalyzation [7,21].
(ii) A linear sweep up (LSU) catalyzation, consisting of a transverse magnetization preparation only [6,22].
(iii) An LSU catalyzation with a binomial RF pulse and spoiler gradient for preparing the longitudinal magnetization (LSU binomial [LSUB]) [8,23]. See Fig. 1 for an illustration.

The combination of these catalyzation sequences with each MOLLI scheme led to a total of 13 different MOLLI setups. Furthermore, each catalyzation sequence was tested with 4, 7, 10 and 13 startup echoes; in total, 12 different catalyzation sequences were compared.

2.1.1. Simulations

While there is an analytical solution for steady-state free-precession [20], there is no equivalent for MOLLI's single-shot bSSFP approach, so this was simulated numerically. Scripts were written using MATLAB 2012a (The MathWorks, Natick, MA, USA), approximating the action of a set of RF pulses on a set of simulated magnetic moments using solutions to the Bloch equations in the rotating frame [24]. See Fig. 2 for a flowchart illustrating the structure of the numerical simulation. Gradient, RF and timing parameters were imported from Philips' pulse programming environment (Philips Healthcare, Best, The Netherlands) to replicate the *in vitro* and *in vivo* MOLLI protocols described here. The imaging slice profile was measured, and replicated in the simulation, and different k-space trajectories were approximated using different timings for the observation window: the first readout TR interval for centric-ordered MOLLI, and the middle readout TR interval for linear-ordered MOLLI. As this simplified approach rendered centric and centric-paired readouts effectively identical, centric-paired ordering was not investigated via simulations. A set of reference T_1 values, corresponding to the seven calibrated phantoms, was estimated with each MOLLI variant by applying a three-parameter Levenberg–Marquardt curve fit to the simulated magnetization measured by each variant, as follows:

$$M(t) = A - B\exp\left(-t/T_1^*\right) \tag{1}$$

where M(t) is the magnetization at time t and $T_1{}^*$ is the "apparent" T_1. Look–Locker correction [11] was then used to correct $T_1{}^*$ to "true" T_1 using as follows:

$$T_1 = T_1^*(B/A - 1) \tag{2}$$

Note that the Look–Locker correction was derived for, and assumes, a spoiled GRE sequence with low flip angle alpha pulses [11]. The approach for T_1 fitting described here is the same as that used in the original MOLLI implementation [1].

For assessment of T_1 measurement accuracy and precision, a Monte Carlo algorithm was written whereby Gaussian noise was added to the MOLLI-measured signal, and T_1 measurements were repeated for low (10:1), medium (30:1), and high (60:1) SNR over 100 noise realizations.

2.1.2. In vitro experiments

In vitro, the four MOLLI variant schemes were compared to conventional MOLLI in the 7 calibrated phantoms, and each variant was tested with all 12 configurations of the catalyzation sequences. T_1 maps were calculated automatically during image reconstruction and T_1 means and standard deviations were measured using regions of interest (ROIs) drawn in ImageJ (National Institutes of Health, Bethesda, MD, USA).

2.1.3. In vivo experiments

Ten healthy volunteers were recruited for this study (mean age [range] = 33 [20–47] years, mean resting heart rate [SD] = 63 [6] bpm). Informed consent was obtained from all participants, and ethical approval was granted by the local ethics committee. For each volunteer, single slice mid-ventricular short axis MOLLI images were acquired using each MOLLI sequence, and myocardial T_1 maps were generated automatically. In order to evaluate the degree of B_1 transmit variation across the heart, B_1+ maps were also acquired. These were obtained using the saturated double angle acquisition method, [25] with an echo-planar imaging readout, [17] a saturation delay of 500 ms, TR = 1 beat, TE = 3.4 ms and an in-plane resolution of 5×10 mm.

To obtain T_1 measurements, myocardial ROIs were drawn on all T_1 maps using ImageJ, and eroded by one pixel to avoid partial volume and chemical shift artifacts at myocardial interfaces. A second ROI was drawn in the center of the cavity to assess blood T_1. Average T_1 values and standard deviations were then measured for each ROI.

2.2. T_1 measurement accuracy

The T_1 measurement accuracy of each MOLLI sequence was evaluated in simulations and *in vitro* via comparison of relative bias values, which were given by:

$$RB(\%) = \frac{100}{N}\sum_N \frac{T_{1\ (MEASURED)} - T_{1\ (REF)}}{T_{1\ (REF)}} \tag{3}$$

where $T_{1\ (REF)}$ is the reference T_1, $T_{1\ (MEASURED)}$ is the MOLLI-estimated T_1, and N is the total number of data points—seven in this case, corresponding to the reference T_1 values.

In vivo, given that there was no T_1 reference standard, the T_1 measurement accuracy of each novel MOLLI variant was compared with a typical 3b(3b)3b(3b)5b LSUB MOLLI sequence via Bland–Altman analysis, performed in SigmaPlot (Systat Software, Chicago, IL, USA). Significant differences in the variants' T_1 bias relative to the reference method were investigated with Student's *t*-tests, performed in Microsoft Excel 2007 (Microsoft, Redmond, WA, USA).

2.2.1. Heart rate dependence of MOLLI variants

The dependence of T_1 measurement accuracy on heart rate was investigated in simulations and *in vitro*. In both experiments, T_1 values were estimated with each MOLLI sequence for all 7 reference T_1 values, with simulated heart rates ranging from 40 to 100 bpm, in steps of 10 bpm. Simulation measurements were made without added noise.

2.2.2. Effect of readout flip angle on T_1 measurement accuracy of MOLLI variants

Each of the MOLLI sequences was also tested, in simulations only, for the effect of readout flip angle errors on their T_1 measurement accuracy.

Please cite this article as: Cameron D, et al, Selection of magnetization catalyzation and readout methods for modified Look–Locker inversion recovery: A T_1 mapping primer, Magn Reson Imaging (2015), http://dx.doi.org/10.1016/j.mri.2015.02.004

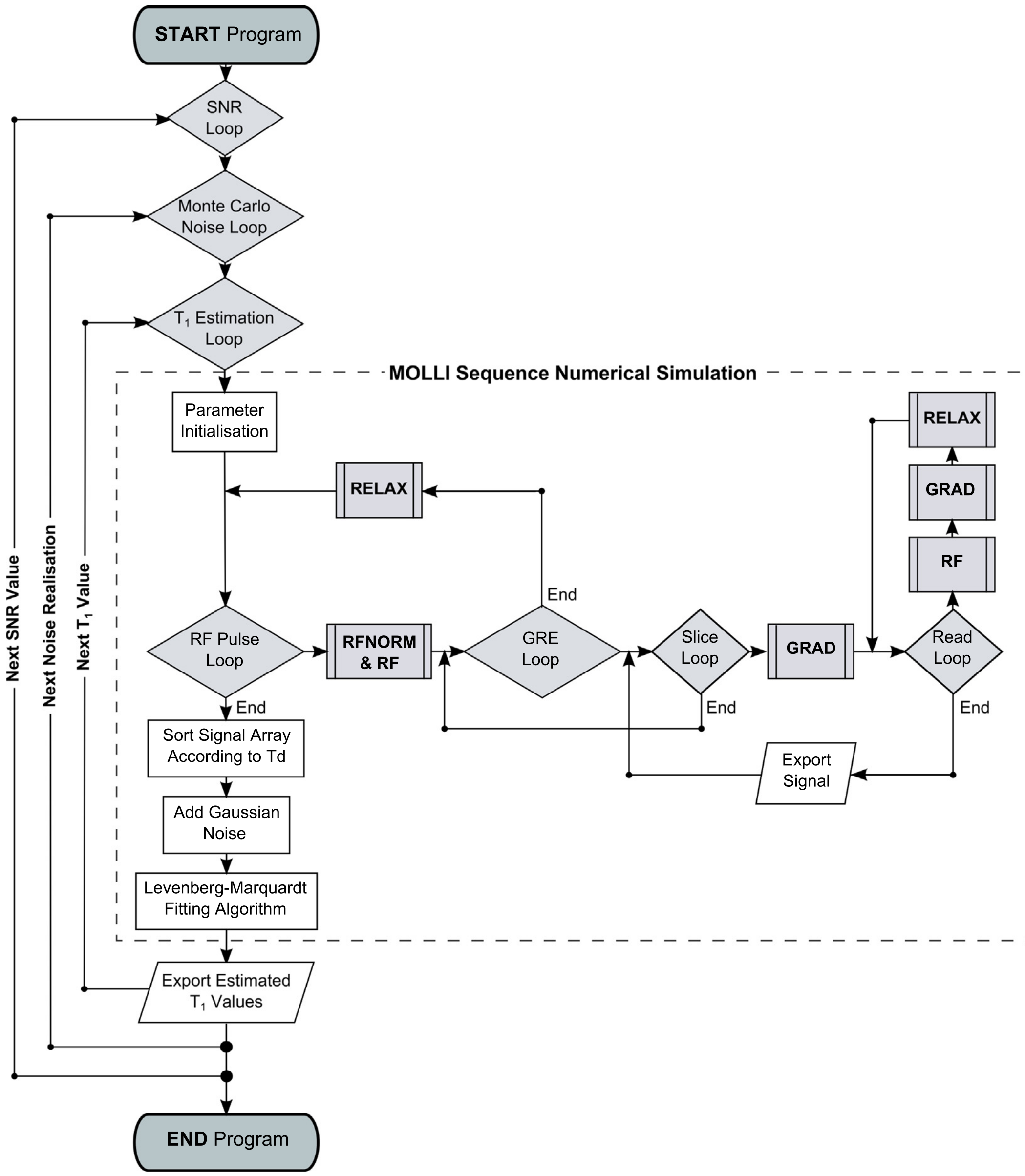

Fig. 2. A simplified flow chart describing the structure of the MOLLI numerical simulation used in this work. Different elements of the pulse sequence are incorporated in a set of nested loops, with the entire numerical simulation being repeated for multiple SNRs (SNR loop), noise realizations (Monte Carlo noise loop), and T_1 values (T_1 estimation loop). Another set of internal loops forms the basis of the MOLLI simulation itself. Starting from the right, the 'read loop' represents a balanced steady-state free-precession (bSSFP) TR interval, containing subroutines corresponding to an alpha pulse (RF), gradients (GRAD) and a short relaxation interval (RELAX). This loop is repeated across a number of isochromats in the read direction, generating a bSSFP signal, and the same process is repeated in the slice direction ('slice loop') to take the slice profile into account. The 'GRE loop' repeats the 'slice' and 'read' loops according the bSSFP train length (i.e. the number of TR intervals), and the outermost 'RF pulse loop' plays the inversion preparation pulse and the magnetization catalyzation pulses. Td = delay time.

A B_1+ error term was introduced to all RF pulses in the readout, with values of −20%, −10%, 0, +10% and + 20% relative to the nominal flip angle. Separate analyses were performed for post-contrast myocardium (470 ms) and native myocardium (1227 ms) T_1 values.

2.3. *T_1 measurement precision*

2.3.1. *Comparison of SNR for all MOLLI variants*

The T_1 estimate precision of each MOLLI sequence, in simulations and *in vivo*, was evaluated via the coefficient of variation (CV):

$$CV(\%) = \frac{\sigma}{\mu} \times 100 \quad (4)$$

a measure of relative dispersion, where σ is the standard deviation and μ is the mean.

In vitro, T_1 estimate precision was assessed via measurement of SNR. This was achieved via an alternative approach whereby the relative SNRs of each variant were compared—since the calculation of the standard deviation of the noise in a phased-array set up is non-trivial when acceleration techniques such as SENSE are used.[26] Signal intensities for each sequence were measured in the MOLLI image with the longest delay time, and noise characteristics were assumed to be the same for each scan, as sequence preparation phases and coil setups were identical throughout. In this way, SNR differences could be evaluated without complex assessment of absolute SNR. *In vivo*, precision was assessed in terms of absolute CV, calculated via Bland–Altman analysis.

Please cite this article as: Cameron D, et al, Selection of magnetization catalyzation and readout methods for modified Look–Locker inversion recovery: A T_1 mapping primer, Magn Reson Imaging (2015), http://dx.doi.org/10.1016/j.mri.2015.02.004

2.4. Contrast-to-noise ratios (CNRs)

CNRs were calculated for each MOLLI variant in simulations, *in vitro*, and *in vivo*, in order to gage the sensitivity of each method to clinically significant T_1 changes: an example of which is that of native T_1 elevation in myocardial edema, as described by Dawson et al. [27] The ability of a T_1 mapping method to differentiate edematous myocardium from normal myocardium can be characterized by the CNR, as follows:

$$CNR = \frac{T_{1(oedema)} - T_{1(normal)}}{\sigma} \quad (5)$$

where $T_{1(\mathrm{normal})}$ and $T_{1(\mathrm{oedema})}$ are the MOLLI-estimated T_1 values in normal myocardium and edematous myocardium, respectively. In this study, the standard deviation of the noise, σ, was assigned a value of unity: given the well-characterized noise in simulations, and the identical scan preparations and receiver bandwidths *in vitro* and *in vivo*. In simulations and *in vitro*, $T_{1(\mathrm{oedema})}$ was represented by the 1227 ms phantom, while the 1110 ms phantom was chosen to represent normal myocardium, $T_{1(\mathrm{normal})}$. *In vivo*, no participants exhibited myocardial edema; therefore, the spleen was used as a surrogate for edematous myocardium, given its comparable T_1 and T_2 relaxation times ($T_1 \approx 1300$ ms and $T_2 \approx 60$ ms at 3 T) [28]. Contrast-to-noise ratio was again calculated using Eq. 5, with $T_{1(\mathrm{oedema})}$ being measured from an additional ROI drawn in the spleen. This analysis was performed in five volunteers, and means and standard deviations were determined.

2.5. Image quality

In order to evaluate T_1 map quality *in vivo*, χ^2 maps were generated offline using Philips' RelaxMaps tool. These indicate how well the data conform to the model used to create the fit. They were assessed subjectively—in parallel with T_1 maps and source images—and image sets that exhibited artifact (pixel-fit failures, bSSFP banding, partial volume, phase wrap) were scored according to the size of the artifacts (0 = no artifact; 1 = subtle artifact, such as local pixel-fit failures; 2 = moderate artifact, obscuring either myocardium or blood pool; 3 = severe artifact, obscuring myocardium and blood pool).

3. Results

3.1. T_1 measurement accuracy

Table 1 shows mean relative bias values for MOLLI sequences in simulations and *in vitro*. Results are summarized for several catalyzation sequences, each with a number of different startup train lengths. The 5b(3b)3b LSU scheme gave the least bias in simulations, while the spoiled GRE scheme gave the least bias *in vitro*. A more detailed breakdown of T_1 measurement accuracy is given in Fig. 3, where relative bias values are shown for individual T_1 values at three different SNRs. This clearly illustrates the tendency for MOLLI sequences to underestimate longer T_1 values, and also shows that estimates of short, post-contrast T_1 values are typically the most sensitive to noise.

3.1.1. Bias of MOLLI variant T_1 measurements in vivo

In vivo, given that the effect of changing the startup train length was minimal both in simulations and *in vitro*, a ten-startup-echo scheme was chosen for each MOLLI variant as a compromise between T_1 measurement accuracy and readout train length. Table 2 shows the T_1 bias, in milliseconds, determined from Bland–Altman analysis, where 3b(3b)3b(3b)5b LSUB MOLLI was used as the reference standard. A positive bias indicates less T_1 underestimation than conventional MOLLI, which is known to substantially underestimate T_1 in native myocardium and blood. In myocardium and blood pool, all MOLLI variants showed similar accuracy to conventional MOLLI, except spoiled GRE MOLLI, which showed a significant positive T_1 bias in myocardium ($p \ll 0.001$). The 5b(3b)3b MOLLI sequence agreed well with conventional MOLLI, with a small bias and a line of zero difference within the 95% confidence intervals of the bias (−17 to 35 ms). Regarding magnetization catalyzation approaches, both LSU-prepared conventional MOLLI and HA-prepared MOLLI showed significantly better T_1 measurement accuracy than the LSUB-prepared reference standard in myocardium ($p = 0.006$ for each).

Table 1
Mean relative bias of MOLLI T_1 estimates in simulations and *in vitro* using different readout schemes and startup train lengths.

	Simulation				*In vitro*			
# Startup echoes	4	7	10	13	4	7	10	13
3b(3b)3b(3b)5b LSUB	13.3	13.0	*12.8*	13.0	**16.8**	17.9	18.0	17.6
3b(3b)3b(3b)5b LSU	11.1	11.2	*11.0*	11.1	17.6	17.5	17.2	*17.1*
3b(3b)3b(3b)5b HA	*10.8*	11.0	10.9	11.3	17.4	17.2	17.2	*17.1*
5b(3b)3b LSUB	9.7	9.7	*9.6*	9.7	19.6	*19.6*	20.0	19.6
5b(3b)3b LSU	9.0	**8.9**	9.3	9.2	19.7	19.6	*19.5*	19.6
5b(3b)3b HA	*8.8*	9.3	9.2	9.4	*19.3*	19.3	19.4	19.4
Spoiled GRE	*9.5*	9.6	9.8	10.0	17.0	17.1	*16.8*	16.9
Centric LSUB	11.6	11.4	*10.4*	11.0	20.4	21.0	21.0	*20.2*
Centric LSU	12.0	11.8	11.6	*9.9*	22.2	21.9	*21.1*	22.5
Centric HA	11.5	11.2	10.9	*10.6*	21.5	21.0	20.4	*20.4*
C-P LSUB	-	-	-	-	18.0	*17.7*	18.5	18.2
C-P LSU	-	-	-	-	*18.2*	18.3	18.3	18.2
C-P HA	-	-	-	-	18.0	*17.7*	18.2	18.0

Inversion recovery fast-spin-echo T_1 measurements are used as comparators, with relative, unsigned biases (%) averaged across all seven reference T_1 values. The lowest mean relative bias for each sequence is highlighted in italics, and the sequences with the overall smallest bias in simulations and in vitro are also indicated in bold. The simulation results shown here were acquired with infinite signal-to-noise.

3.1.2. Heart rate dependence of MOLLI variants

Figs. 4 and 5 show the heart rate dependence of each MOLLI sequence—in simulations and *in vitro*, respectively—with percentage T_1 estimate error plotted against reference T_1 values. In simulations only, linear and centric sequences were applied with all three catalyzation approaches (LSU, LSUB, and HA, ten startup echoes) without added Gaussian noise. Both in simulations and *in vitro*, 5b(3b)3b MOLLI overestimated short T_1 values at low heart rates, but otherwise underestimated T_1. All other variants underestimated T_1 at all heart rates, and the underestimation increased with increasing heart rate. Spoiled GRE MOLLI showed the least heart rate dependence *in vitro* (mean T_1 estimate error [SD] = −15.3 [5.0] %); while centric MOLLI showed the greatest dependence (mean T_1 measurement error [SD] = −21.4 [8.0] %).

3.1.3. Effect of readout flip angle on T_1 measurement accuracy of MOLLI variants

Fig. 6A shows plots of T_1 measurement error versus flip angle error for each MOLLI variant. Conventional MOLLI schemes showed the greatest T_1 variation with flip angle, particularly with LSUB and HA catalyzations, where T_1 errors reached 6.4% and 7.0%, respectively. The LSU-prepared variant showed substantially less flip angle dependence, (max. T_1 error = 2.7%) and was more consistent across post-contrast myocardium, native myocardium and blood-like T_1 values. Centric MOLLI schemes gave T_1 estimates that were less flip-angle-dependent than conventional MOLLI (max. T_1 errors = 0.7% for LSUB, 0.9% for LSU, and 1.5% for HA) as did 5b(3b)3b-LSU and spoiled GRE MOLLI (max. T_1 errors = 3.5% and 1.1%, respectively). In general, T_1 estimates were seen to decrease with increasing flip angle; however, LSUB-prepared

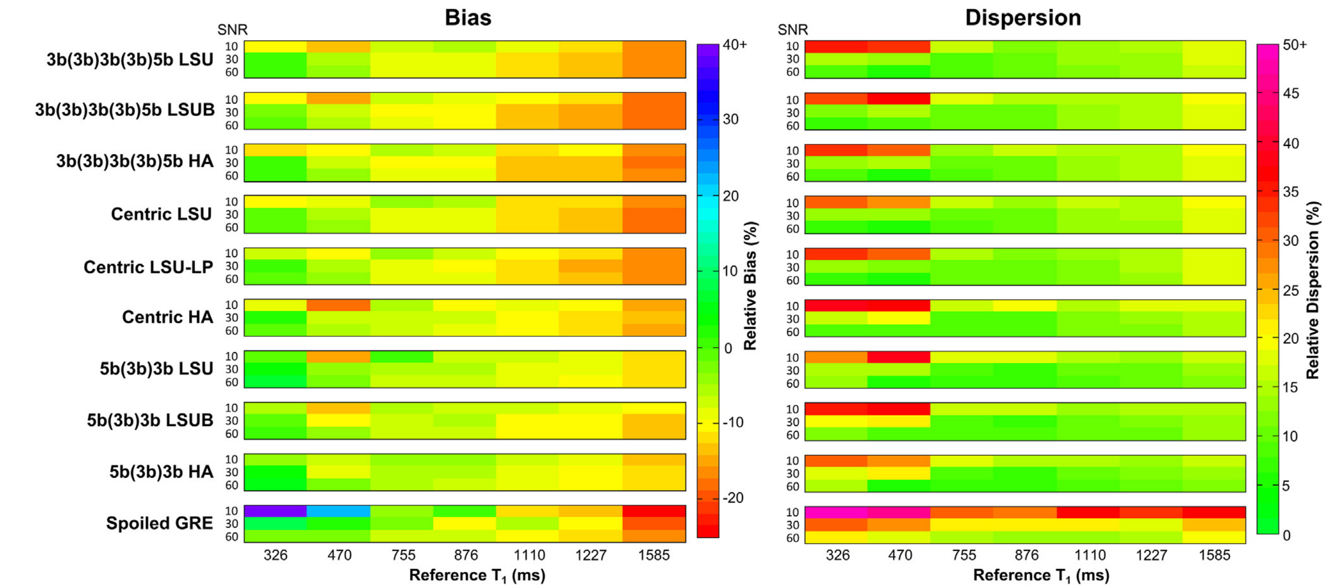

Fig. 3. Plots of the bias and dispersion of MOLLI variant T_1 measurements from Monte Carlo simulations: The relative bias and relative dispersion of ten MOLLI sequences are shown using color scales, which are limited to +40% and +50%, respectively—in order to highlight differences between the methods. Results were obtained from 100 noise realizations at SNRs of 10, 30, and 60.

centric MOLLI gave post contrast T_1 estimates that increased with flip angle. *In vivo*, B_1+ maps gave a mean (SD) flip angle of 87.4 (11.9)% of the nominal value across the left ventricle. Fig. 6B shows an example of an axial B_1+ map acquired in a volunteer.

3.2. T_1 measurement precision

3.2.1. Comparison of SNR for all MOLLI variants

Measurements of T_1 estimate precision from simulations are shown in Table 3, with a detailed illustration in Fig. 2. Mean relative dispersions are similar from sequence-to-sequence, tending to decrease with increasing SNR. The 5b(3b)3b sequences demonstrated the smallest mean relative dispersions, while spoiled GRE MOLLI showed significantly larger mean relative dispersions than all other variants at all SNRs ($p \ll 0.001$ in all cases). Furthermore, estimates of short, post-contrast-like T_1 values were seen to be the most variable in cases of poor SNR (10:1).

In vitro pseudo-SNR measurements were made with an assumed noise of unity, because of the identical sequence preparation phases and coil setups used, i.e. the signal itself was taken as a measure of SNR, after correction for scaling factors associated with digital imaging and communications in medicine (DICOM) storage. Table 2 shows pseudo-SNR measurements for all MOLLI variant/startup combinations. Centric MOLLI gave the best SNR, and the LSU catalyzation was associated with improved SNR in all variants. The spoiled GRE variant showed the poorest SNR.

Table 2
Bland–Altman T_1 bias and dispersion (CVs) for MOLLI sequences in myocardium and blood, *in vivo*.

	Myocardium		Blood pool	
MOLLI sequence	T_1 bias (SD) ms	Mean CV	T_1 bias (SD) ms	Mean CV
3b(3b)3b(3b)5b LSUB	-	0.132	-	0.019
3b(3b)3b(3b)5b LSU	66 (35)*	0.027*	−9 (20)	0.020
3b(3b)3b(3b)5b HA	64 (36)*	0.104	6 (39)	**0.017**
5b(3b)3b LSUB	9 (35)	0.133	**49 (31)**	0.020
5b(3b)3b LSU	75 (46)*	0.038*	31 (24)	0.039*
5b(3b)3b HA	70 (46)*	0.030*	31 (35)	0.039*
Spoiled GRE	**97 (57)***	0.153	−28 (63)	0.044*
Centric LSUB	−31 (65)	0.115	−26 (59)	0.032*
Centric LSU	21 (64)	0.041*	−28 (110)	0.071*
Centric HA	37 (46)	**0.027***	−5 (105)	0.060*
C-P LSUB	−39 (78)	0.119	−39 (54)	0.044*
C-P LSU	29 (45)	0.037*	−66 (45)*	0.049*
C-P HA	14 (59)	0.029*	−42 (80)	0.049*

A 3b(3b)3b(3b)5b LSUB MOLLI sequence is given as the reference standard for Bland–Altman analysis. The best accuracy (positive bias indicating less T_1 underestimation relative to conventional MOLLI) and precision are indicated in bold for T_1 measurements in myocardium and blood pool.

* Indicates a significant difference relative to the reference—3b(3b)3b(3b)5b LSUB MOLLI, relevant p-values in text.

3.2.2. Relative dispersion of MOLLI variant T_1 measurements in vivo

Table 2 shows measures of MOLLI variant precision *in vivo*, quoted as CVs. Spoiled GRE MOLLI and centric and centric-paired variants showed significantly poorer precision than conventional MOLLI in myocardium ($p \ll 0.001$, $p = 0.003$ and $p = 0.001$, respectively), while 5b(3b)3b MOLLI showed similar precision to the conventional sequence. HA and LSU-prepared MOLLI variants tended to show significantly improved precision over conventional MOLLI. In blood pool, all non-3b(3b)3b(3b)5b MOLLI sequences—aside from 5b(3b)3b LSUB MOLLI—showed significantly reduced precision relative to conventional MOLLI ($p < 0.05$ for all).

3.3. Contrast-to-noise ratios

Table 4 collates pseudo-CNRs from simulations, *in vitro* experiments, and *in vivo* experiments. Both in simulations and *in vivo*, 5b(3b)3b LSU MOLLI showed the largest CNR, closely followed by the 3b(3b)3b(3b)5b LSU sequence; furthermore, the CNR of 5b(3b)3b LSU MOLLI showed the least variability *in vivo*. Considering *in vitro* data, MOLLI sequences with the 3b(3b)3b(3b)5b sampling scheme showed slightly higher CNRs than those with the 5b(3b)3b scheme, while spoiled GRE MOLLI demonstrated the largest CNR.

3.4. Image quality

Considering *in vitro* image quality, Fig. 7 illustrates signal intensity variations in phantoms according to k-space trajectory. Linear ordering produces slightly uneven signal intensity in MOLLI

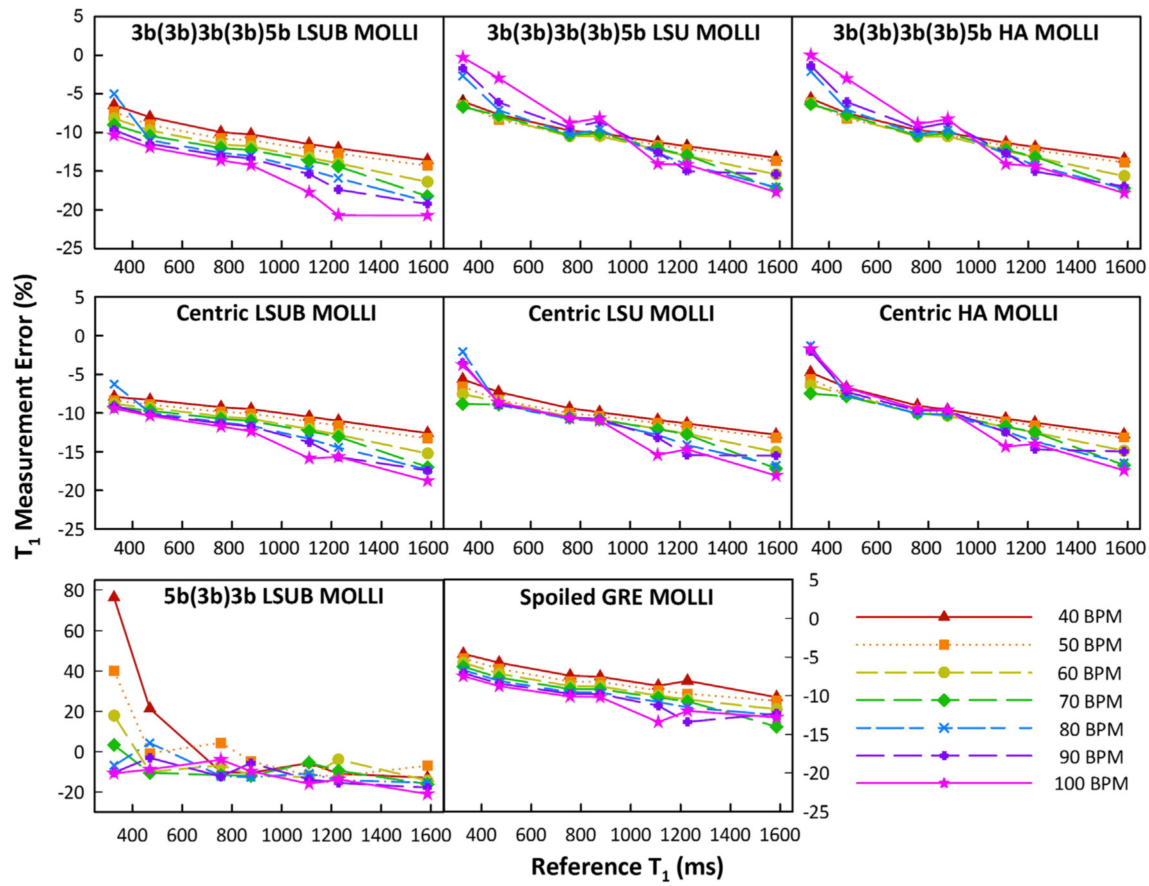

Fig. 4. Plots showing the heart rate dependence of MOLLI variants in simulations: Percentage T_1 measurement error in conventional and centric MOLLI variants is plotted against virtual phantom T_1 values in each pane. Data are shown for simulated heart rates of 40 bpm–100 bpm. GRE = gradient recalled echo, LSU = linear sweep up, LSUB = LSU binomial, and HA = half-alpha.

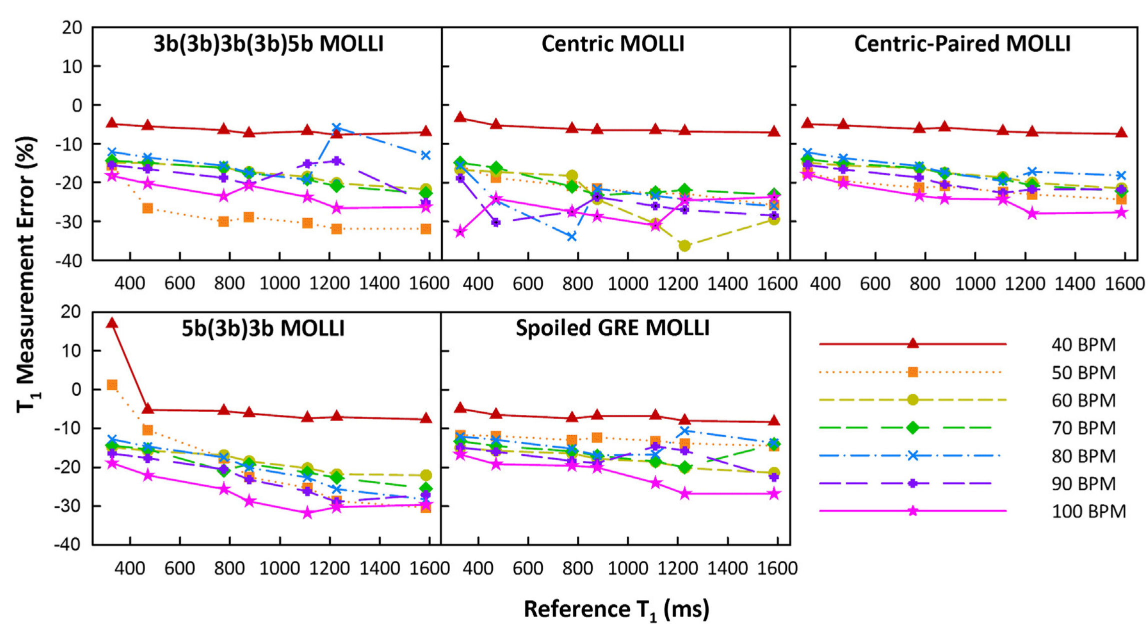

Fig. 5. Plots showing the heart rate dependence of conventional MOLLI and five MOLLI variants in vitro: Each variant uses a ten startup echo LSU catalyzation sequence. Percentage T_1 measurement error is plotted against IR fast-spin-echo reference T_1 values in each. Data are shown for simulated heart rates of 40 bpm–100 bpm. GRE = gradient recalled echo.

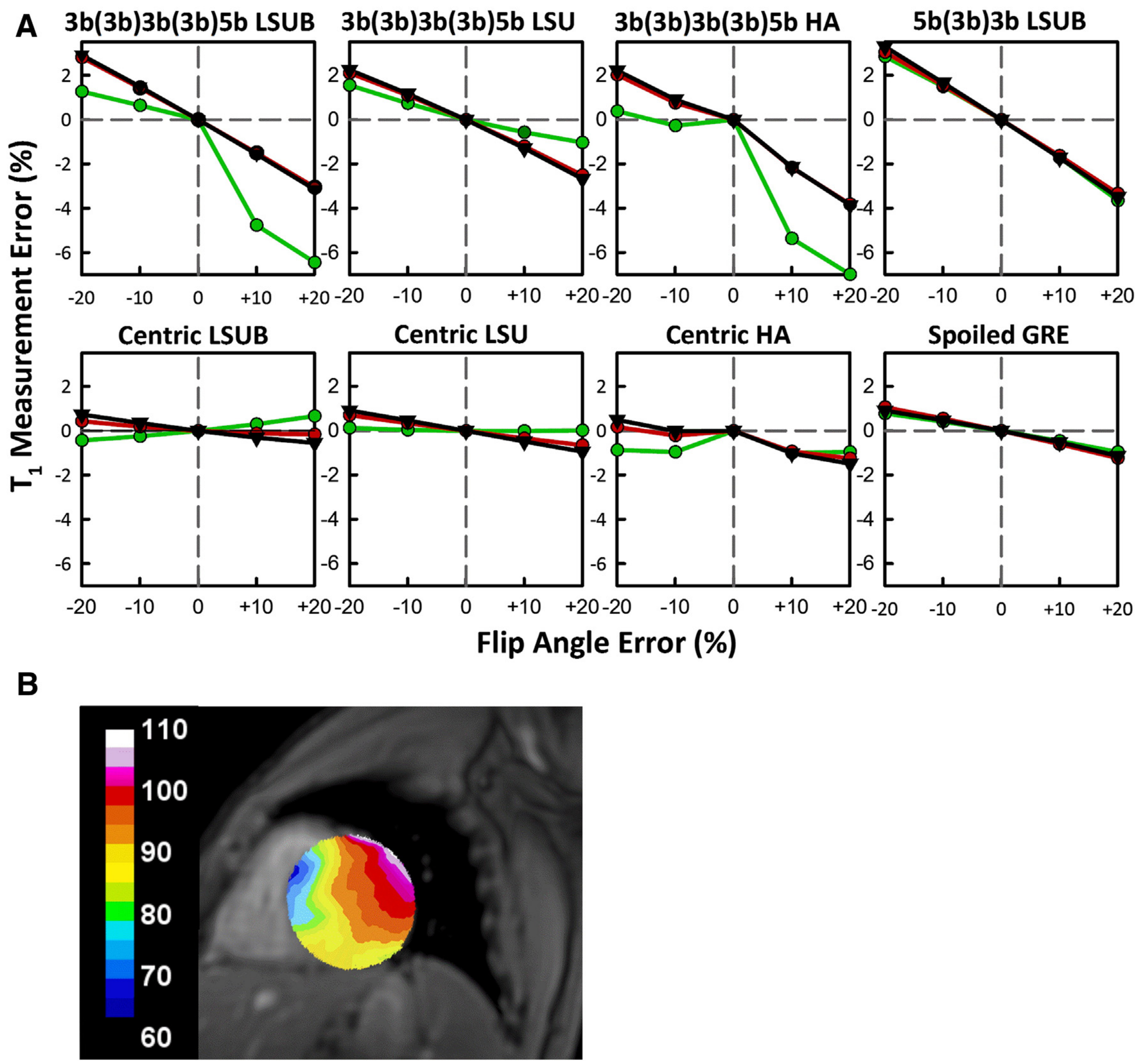

Fig. 6. The effect of flip angle error on MOLLI variant T_1 measurement accuracy in simulations: Plots show T_1 measurement errors in each MOLLI variant for flip angle errors of −20%, −10%, 0, + 10% and +20% (A). Colored lines indicate errors for post-contrast myocardium (470 ms, green), native myocardium (1227 ms, black), and blood-like (1585 ms, red) T_1 values; GRE = gradient recalled echo, LSU = linear sweep up, LSUB = LSU binomial, and HA = half-alpha. Also shown is a short-axis localizer image with a color overlay showing the relative B_1 across the left ventricle (B).

Table 3
Relative dispersion and SNR measurements for each set of MOLLI variants and catalyzation sequences in simulations and in vitro.

MOLLI variant/ catalyzation	Simulation - mean relative dispersion (%)			*In vitro* pseudo-SNR
	SNR = 10:1	SNR = 30:1	SNR = 60:1	
3b(3b)3b(3b)5b LSUB	21.3	13.5	11.7	309.0
3b(3b)3b(3b)5b LSU	20.4	13.0	10.7	367.6
3b(3b)3b(3b)5b HA	20.5	13.4	11.2	363.1
5b(3b)3b LSUB	21.5	13.1	10.0	360.7
5b(3b)3b LSU	20.6	**11.0**	**9.0**	367.6
5b(3b)3b HA	**19.2**	12.8	9.3	304.9
Spoiled GRE	41.8	23.2	16.2	80.3
Centric LSUB	19.6	12.9	10.9	505.8
Centric LSU	19.5	12.9	10.9	530.8
Centric HA	22.8	13.3	10.2	**532.6**
C-P LSUB	-	-		408.9
C-P LSU	-	-		484.8
C-P HA	-	-		456.9

Data are presented for simulations (mean CVs in percent) and for in vitro experiments (pseudo SNR measurements). Sequences with the best CV/SNR are indicated in bold. C-P = centric-paired.

base images, centric ordering leads to large, eddy-current-induced signal intensity variations across the image, and centric-paired ordering gives smooth signal intensity.

Example T_1 maps for all MOLLI schemes applied *in vivo* are displayed in Fig. 8. In total, 111 out of 130 T_1 maps exhibited artifacts to some degree. Centric and centric-paired MOLLI readouts showed significantly worse artifact scores than linear 3b(3b)3b(3b)5b MOLLI (mean [SD] = 2.1 [1.0] for both, versus 1.0 [0.7], $p \ll 0.001$) and demonstrated considerable blurring and poor χ^2. The 5b(3b)3b MOLLI variant had similar artifact scores to conventional MOLLI (mean [SD] = 1.2 [0.8]), as did spoiled GRE MOLLI—which gave noisy T_1 and χ^2 maps, but exhibited no prominent artifacts (mean [SD] score = 1.2 [0.4]). In terms of catalyzation sequences, LSU demonstrated significantly better artifact scores than LSUB (mean [SD] = 1.0 [0.1] versus 2.0 [0.7], p = 0.0002); HA-catalyzed MOLLI sequences had similar artifact scores to those catalyzed by LSUB.

4. Discussion

The main findings of this work are as follows: 1) the LSU magnetization catalyzation sequence yields substantially better T_1

Table 4
CNRs for each set of MOLLI variants and catalyzation sequences in simulations, *in vitro*, and *in vivo*.

MOLLI variant/catalyzation	Simulations	*In vitro*	*In vivo*
3b(3b)3b(3b)5b LSUB	80.3	109.5	116.1 (81.6)
3b(3b)3b(3b)5b LSU	90.3	104.7	181.9 (50.2)
3b(3b)3b(3b)5b HA	92.0	101.9	126.2 (161.9)
5b(3b)3b LSUB	97.5	97.1	127.7 (162.5)
5b(3b)3b LSU	**106.9**	91.1	**188.8 (45.0)**
5b(3b)3b HA	91.8	92.7	167.6 (74.5)
Spoiled GRE	51.6	**127.5**	136.4 (42.8)
Centric LSUB	70.7	72.1	131.9 (82.3)
Centric LSU	83.0	69.3	147.7 (92.0)
Centric HA	91.1	61.0	103.7 (95.7)
C-P LSUB	-	109.2	175.5 (117.3)
C-P LSU	-	98.4	149.9 (124.1)
C-P HA	-	100.4	179.7 (45.2)

Data are shown for simulations, *in vitro* experiments, and *in vivo* experiments. Simulation and *in vitro* results indicate the difference in T_1 estimates between 'abnormal myocardium' (a phantom with $T_1 = 1227$ ms) and 'healthy myocardium' (a phantom with $T_1 = 1110$ ms). *In vivo* results are presented as mean (SD), and represent the difference between 'abnormal myocardium' (spleen is used as a surrogate, with $T_1 \approx 1300$ ms) and healthy myocardium. In all instances, the standard deviation of the noise is assumed to be unity, and the sequences with the best CNR are indicated in bold. C-P = centric-paired.

measurement accuracy versus the LSUB catalyzation in myocardium, being less sensitive to B_1+ inhomogeneity, less heart-rate-dependent, and giving better SNR and CNR; 2) 5b(3b)3b MOLLI shows similar T_1 measurement accuracy and precision to conventional MOLLI, with a reduced acquisition time and modestly improved CNR, but it was seen to overestimate short T_1 values at low heart rates; 3) spoiled GRE MOLLI showed the least heart rate dependence, and improved T_1 measurement accuracy in myocardium, yet it was also the most sensitive to noise; 4) centric and centric-paired MOLLI variants do not show significantly improved T_1 measurement accuracy or precision over conventional MOLLI with a linear k-space trajectory, and are associated with increased image artifact *in vivo*.

Generally, the numerical simulation was a good predictor of *in vitro* and *in vivo* results. Phantom measurements were in concordance with those calculated in simulations, though heart-rate dependence was more pronounced *in vitro* for all variants. Considering the performance of MOLLI variants *in vitro* and *in vivo*, both centric and centric-paired MOLLI variants' T_1 estimates showed reduced accuracy versus conventional MOLLI *in vitro*, and increased image artifact *in vivo*. Both effects were likely due to transient signal oscillations during the approach to the steady state. Overall, the T_1 measurement accuracy of these variants was similar to that of conventional MOLLI, albeit with poorer T_1 map quality.

The 5b(3b)3b MOLLI sequence performed well both *in vitro* and *in vivo*, demonstrating similar T_1 measurement accuracy, precision, and SNR to conventional MOLLI, despite having a much shorter acquisition duration. It was less sensitive to B_1+ inhomogeneity and the quality of its T_1 maps was comparable with conventional MOLLI maps, showing very few visible artifacts. Furthermore, it showed increased CNR relative to conventional MOLLI both in simulations and *in* vivo, indicating improved sensitivity to T_1 changes in myocardial edema. The 5b(3b)3b scheme should perform well in patients who find breath-holding difficult; however, it was seen to overestimate shorter T_1 values at low simulated heart rates in simulations and *in vitro*, and is thus recommended for native T_1 mapping only—concurring with recommendations made by the scheme's inventors [15].

Regarding magnetization catalyzation sequences, the LSU catalyzation performed best for all bSSFP MOLLI sequences: it gave the largest SNR *in vitro*; good CNR across the board; excellent T_1 map quality and precision *in vivo*; superior T_1 measurement accuracy to LSUB-prepared MOLLI in myocardium; and less sensitivity to B_1+ inhomogeneity. HA-prepared MOLLI schemes showed similar T_1 measurement precision to LSU-prepared schemes, better accuracy than conventional LSUB-prepared MOLLI for myocardial T_1 measurements, and better SNR, but they were associated with greater artifact-incidence than LSU-prepared sequences and demonstrated substantial T_1 measurement errors in the presence of B_1+ inhomogeneity. In terms of heart rate dependence, LSU-prepared MOLLI showed improved T_1 measurement accuracy over LSUB-prepared schemes in simulations; due, in part, to the fact that longitudinal recovery is retarded by the addition of the binomial pulse catalyzation. Furthermore, between the two composite RF pulse elements of the longitudinal preparation, the magnetization is dephased before being restored to the z-axis—increasing the influence of off-resonance on T_1 measurement accuracy. Due to the large range of off-resonance frequencies in the heart, [19] this will cause substantial dephasing across the left ventricle and reduce the magnitude of the longitudinal magnetization, as well as overall SNR, for the LSUB-catalyzed MOLLI sequence. It should also be noted that large and variable T_1 estimate errors were seen with an LSUB catalyzation when a B_1+ error was introduced. Bearing these considerations in mind, we recommend an LSU catalyzation sequence for use with MOLLI T_1 mapping.

Spoiled GRE MOLLI showed less heart rate dependence than the other schemes *in vitro*, as well as superior CNR, but it gave poor blood pool T_1 measurements *in vivo*. This can be partly explained by its poor SNR, which was demonstrated in simulations and *in vitro*; however, a more likely source of error is the lack of intrinsic flow-compensation in spoiled GRE, which results in reduced signal intensity in flowing blood [29]. Thus, spoiled GRE MOLLI schemes are not recommended for myocardial T_1 mapping.

Additional work is required to understand the effect of off-resonance on transient signal oscillations and, thus, on the performance of catalyzation

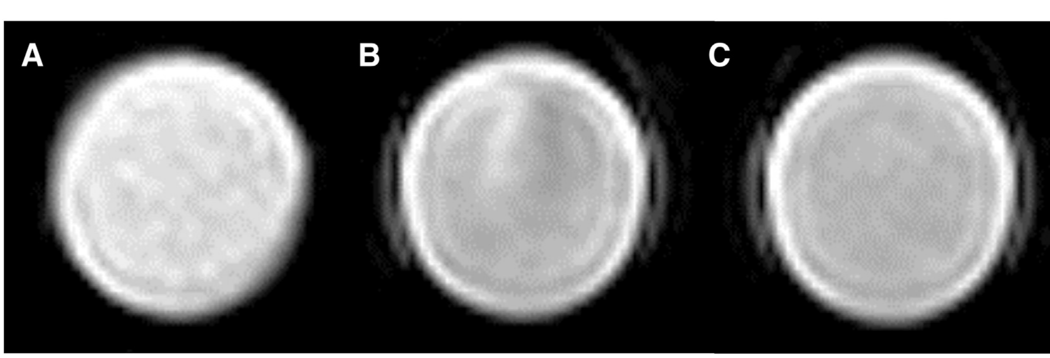

Fig. 7. Magnitude images from phantoms scanned with different MOLLI k-space trajectories: A) – linear; B) – centric; and C) – centric-paired. Note that centric-paired MOLLI gives smooth signal intensity without the large variations seen with centric ordering.

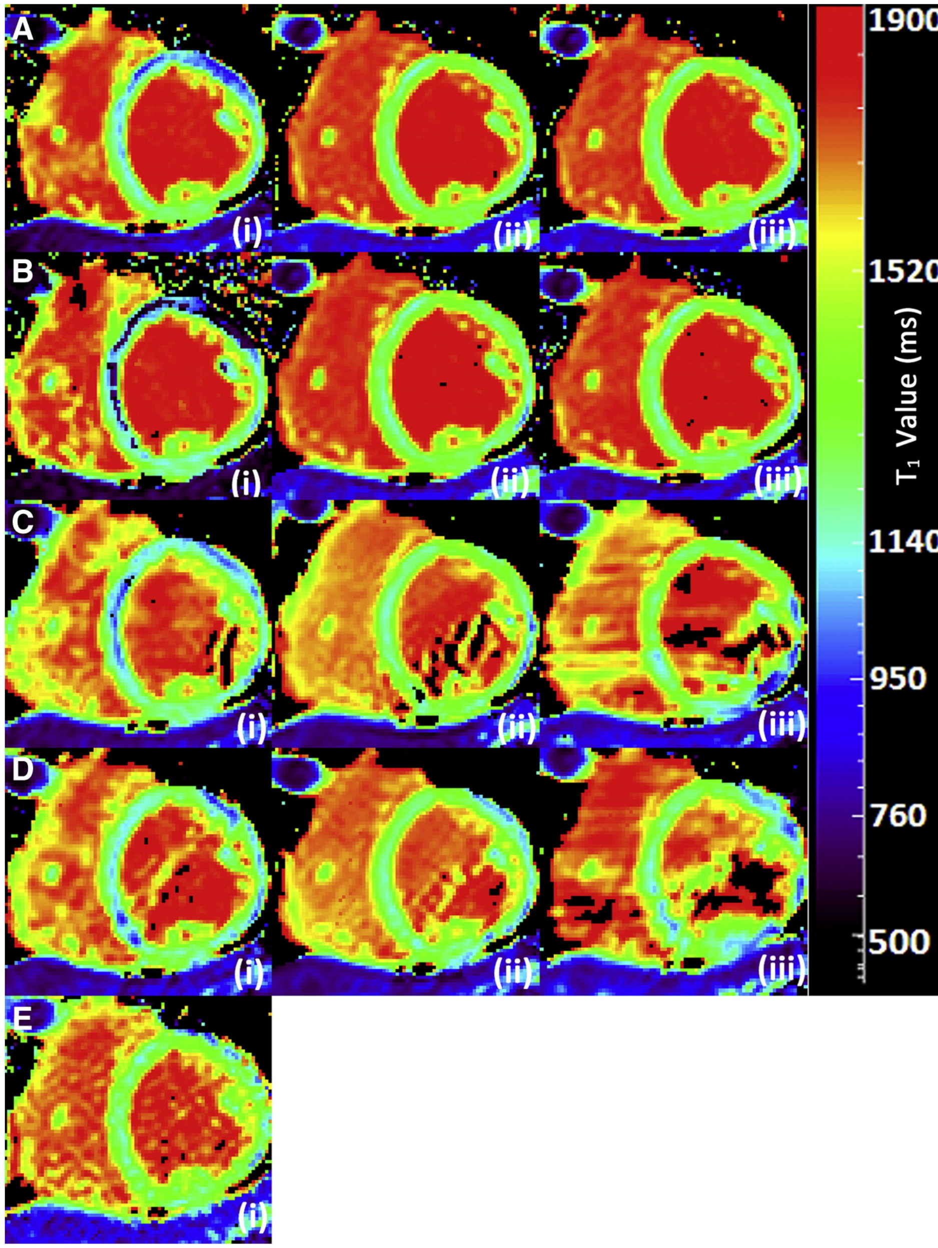

Fig. 8. Examples of in vivo short axis cardiac T_1 maps acquired in one volunteer: Five groups of MOLLI variants are used: A) conventional 3b(3b)3b(3b)5b; B) 5b(3b)3b; C) centric; D) centric-paired; and E) spoiled GRE. Numerals denote different catalyzation sequences, each using 10 startup echoes: (i) LSU; (ii) LSU (skipped pulse pair); and (iii) half-alpha. The color scale on the right describes the range of T_1 values shown in these T_1 maps, in ms.

methods for T_1 mapping. In addition, simulated MOLLI base images should be generated for a better understanding of the effect of catalyzation methods or readout sequences on image quality [30]. Further to the MOLLI variants studied in this work, a preliminary study included a variant with a steady-state free-precession free induction decay readout sequence, as described by Bernstein [29]. This scheme was not investigated further, due to substantial blood pool artifacts stemming from its unbalanced gradient configuration.

5. Conclusions

This study, the first comprehensive investigation of magnetization catalyzation schemes in T_1 mapping, highlights the significance of transient signal oscillations in T_1 mapping, and indicates a number of areas where the MOLLI acquisition setup can be improved. Most significantly, we have shown that an LSU catalyzation sequence gives the best MOLLI T_1 measurement accuracy and precision, as well as T_1 map quality. Finally we confirmed that 5b(3b)3b MOLLI agrees well with conventional MOLLI: offering robust native T_1 measurements in 11 heartbeats, which will benefit patients who cannot tolerate long breath-holds.

Authors' information

Dana K. Dawson and Thomas W. Redpath are joint senior authors.

Acknowledgments

Thanks are due to Richard G. Spencer, for his helpful insights on the topics discussed in this work, to James Hutchison and Che Ahmad Azlan, for providing the basic building blocks of the numerical simulations, and to Rebecca Colleran, for assisting with pilot studies.

References

[1] Messroghli DR, Radjenovic A, Kozerke S, Higgins DM, Sivananthan MU, Ridgway JP. Modified Look-Locker inversion recovery (MOLLI) for high-resolution T1 mapping of the heart. Magn Reson Med 2004;52:141–6.
[2] Messroghli DR, Greiser A, Fröhlich M, Dietz R, Schulz-Menger J. Optimization and validation of a fully-integrated pulse sequence for modified look-locker inversion-recovery (MOLLI) T1 mapping of the heart. J Magn Reson Imaging 2007;26:1081–6.
[3] Higgins DM, Moon JC. Review of T1 mapping methods: comparative effectiveness including reproducibility issues. Curr Cardiovasc Imaging Rep 2014;7:9252.
[4] Look DC, Locker DR. Nuclear spin-lattice relaxation measurements by tone-burst modulation. Phys Rev Lett 1968;20:987–9.
[5] Oppelt A, Graumann R, Barfuss H, Fischer H, Hartl W, Schajor W. FISP: a new fast MRI sequence. Electromedica 1986;54:15–8.
[6] Deshpande VS, Chung Y, Zhang Q, Shea SM, Li D. Reduction of transient signal oscillations in true-FISP using a linear flip angle series magnetization preparation. Magn Reson Med 2003;49:151–7.
[7] Deimling M, Heid O. Magnetization prepared true FISP imaging. Proceedings of the second annual meeting of ISMRM, 6-12 August, 1994; San Francisco, United States; 1994. p. 495.
[8] Foxall D. Starter sequence for steady-state free precession imaging. Magn Reson Med 2005;53:919–29.
[9] Jung BA, Hennig J, Scheffler K. Single-breathhold 3D-trueFISP cine cardiac imaging. Magn Reson Med 2002;48:921–5.
[10] Bieri O, Markl M, Scheffler K. Analysis and compensation of eddy currents in balanced SSFP. Magn Reson Med 2005;54:129–37.
[11] Deichmann R, Haase A. Quantification of T1 values by SNAPSHOT-FLASH NMR imaging. J Magn Reson 1992;96:608–12.
[12] Gai ND, Stehning C, Nacif M, Bluemke DA. Modified Look-Locker T1 evaluation using Bloch simulations: human and phantom validation. Magn Reson Med 2013;69:329–36.
[13] Haase A, Frahm J, Matthaei D, Hanicke W, Merboldt K. FLASH imaging. Rapid NMR imaging using low flip-angle pulses. J Magn Reson 1986;67:258–66.
[14] Kellman P, Wilson JR, Xue H, Bandettini WP, Shanbhag SM, Druey KM, et al. Extracellular volume fraction mapping in the myocardium, part 2: initial clinical experience. J Cardiovasc Magn Reson 2012;14:64.
[15] Kellman P, Hansen M. T1-mapping in the heart: accuracy and precision. J Cardiovasc Magn Reson 2014;16:2.
[16] Hong K, Kim D. MOLLI and AIR T1 mapping pulse sequences yield different myocardial T1 and ECV measurements. NMR Biomed 2014;27:1419–26.
[17] Mueller A, Kouwenhoven M, Naehle CP, Gieseke J, Strach K, Willinek WA, et al. Dual-source radiofrequency transmission with patient-adaptive local radiofrequency shimming for 3.0-T cardiac MR imaging: initial experience. Radiology 2012;263:77–85.
[18] Krishnamurthy R, Pednekar A, Kouwenhoven M, Cheong B, Muthupillai R. Evaluation of a subject specific dual-transmit approach for improving B1 field homogeneity in cardiovascular magnetic resonance at 3T. J Cardiovasc Magn Reson 2013;15:68.
[19] Kellman P, Herzka D, Arai A, Hansen M. Influence of Off-resonance in myocardial T1-mapping using SSFP based MOLLI method. J Cardiovasc Magn Reson 2013;15:63.
[20] Ernst RR, Anderson WA. Application of Fourier transform spectroscopy to magnetic resonance. Rev Sci Instrum 1966;37:93–102.
[21] Sahar S, Stuber M, Hays AG, Weiss RG, Schär M. Robust volume-targeted balanced steady-state free-precession coronary magnetic resonance angiography in a breathhold at 3.0 tesla: a reproducibility study. J Cardiovasc Magn Reson 2014;16:27.
[22] Weingärtner S, Roujol S, Akçakaya M, Basha TA, Nezafat R. Free-breathing multislice native myocardial T1 mapping using the slice-interleaved T1 (STONE) sequence. Magn Reson Med 2014. http://dx.doi.org/10.1002/mrm.25387.
[23] Peng H, Stoeck CT, Smink J, Peters DC, Ngo L, Goddu B, et al. Noncontrast SSFP pulmonary vein magnetic resonance angiography: impact of off-resonance and flow. J Magn Reson Imaging 2010;32:1255–61.
[24] Bloch F. Nuclear induction. Phys Rev 1946;70:460–74.
[25] Cunningham CH, Pauly JM, Nayak KS. Saturated double-angle method for rapid B1+ mapping. Magn Reson Med 2006;55:1326–33.
[26] Constantinides CD, Atalar E, McVeigh ER. Signal-to-noise measurements in magnitude images from NMR phased arrays. Magn Reson Med 1997;38:852–7.
[27] Dawson DK, Neil CJ, Henning A, Cameron D, Jagpal B, Bruce M, et al. Tako-Tsubo cardiomyopathy: a heart stressed out of energy? J Am Coll Cardiol Img 2014. http://dx.doi.org/10.1016/j.jcmg.2014.10.004.
[28] De Bazelaire CM, Duhamel GD, Rofsky NM, Alsop DC. MR imaging relaxation times of abdominal and pelvic tissues measured in vivo at 3.0 T: preliminary results 1. Radiology 2004;230:652–9.
[29] Bernstein MA. Gradient echo. In: Bernstein MA, King KF, Zhou XJ, editors. Handbook of MRI pulse sequences. Burlington: Elsevier Academic Press; 2004. p. 579–605.
[30] Williams CF, Redpath TW. Sources of artefact and systematic error in quantitative snapshot FLASH imaging and methods for their elimination. Magn Reson Med 1999;41:63–71.